Low-Energy Spiking Neural Network Using $Ge_4Sb_6Te_7$ Phase Change Memory Synapses

Shafin Bin Hamid, Asir Intisar Khan, *Member, IEEE*, Huairuo Zhang, Albert V. Davydov, and Eric Pop, *Fellow, IEEE*

***Abstract*— Spiking neural networks (SNNs) with phase change memory (PCM) devices are promising for in-memory computing, but their performance is often constrained by the abrupt depression (conductance decrease) of PCM synapses. Here, we report an energy-efficient SNN using $Ge_4Sb_6Te_7$ (GST467) as the phase-change material in a *single* device per synapse with *identical* pulses, and find ∼2.5× reduction of inference energy in such SNNs compared to SNNs using two conventional PCMs per synapse. We leverage the unique gradual potentiation and depression characteristics of $Ge_4Sb_6Te_7$ in a behavioral model and train a two-layer SNN to demonstrate both pattern and online learning. We also uncover the trade-offs between energy consumption and SNN recognition rate considering resistance drift and conductance ranges of the synapses, providing a design guideline for future energy-efficient PCM-based SNN.**

***Index Terms*— Phase change memory, spiking neural network, online learning, resistance drift.**

I. Introduction

PHASE change memory (PCM) is a promising candidate for neuromorphic computing [1], [2], [3], [4] because its conductance can be gradually changed using short voltage pulses [2]. PCM devices can be used as synapses in spiking neural networks (SNNs) and could offer an energy-efficient solution to the 'memory wall' problem in conventional von Neumann computing [5]. PCMs can also be fabricated at sufficiently low temperature, to be directly integrated on silicon logic substrates or even flexible electronics [6], [7]. A conventional material for PCM has been $Ge_2Sb_2Te_5$ (GST225), which can be gradually crystallized from its low to high conductance state (potentiation, i.e. 'set'); however, returning the material to its amorphous state occurs with an abrupt drop in conductance (depression, i.e. 'reset') and this transition constrains its use as a synapse [2], [3].

To overcome this, *non-identical* pulses of increasing magnitude can be used to enable gradual conductance change of GST225-based synapses during amorphization [1]. However, such operation requires a 'read-verify' [8] before each synaptic weight update, and generating non-identical pulses also increases system-level complexity. An alternative approach with identical pulse trains employs *two* GST225-PCM devices per synapse, using just their gradual crystallization behaviors [3], [4]. However, using *two* PCM devices for each synapse leads to larger inference energy and lower device density. Moreover, the impact of PCM device non-idealities such as conductance (= 1/resistance) drift [9], [10] on SNNs needs to be understood for performance optimization.

In this work, we demonstrate a two-layer SNN based on a different type of phase change material, $Ge_4Sb_6Te_7$ (GST467). This material enables gradual potentiation and depression with *identical* pulse trains using a *single* PCM device per synapse, a more energy-efficient approach. Employing an experimentally-validated behavioral model, we train our SNN using unsupervised spike-timing dependent plasticity (STDP) [11], [12] and find ∼2.5× reduction in SNN inference energy compared to that with two PCMs per synapse. The impact of drift across various conductance ranges on the SNN inference energy and recognition rate is also explored.

II. Experimental Results and Behavioral Model

Fig. 1(a) shows the schematic of a mushroom cell PCM [∼110 nm bottom electrode (BE) diameter] with GST467 as the phase-change material [13]. Atomic-resolution scanning transmission electron microscopy (STEM) imaging of GST467 reveals SbTe nanocomposite in a GeSbTe (GST) matrix, confirmed by their corresponding fast Fourier transform (FFT) images [**Fig. 1(a)**]. Electrical measurements in **Fig. 1(b)** and **1(c)** show a gradual change in conductance (G) with a ∼10× window for both potentiation (set) and depression (reset). These are achieved with identical pulse trains of 0.72 V amplitude and 1/7/3 ns (rise/width/fall time) during set, and 1.45 V, 1/45/1 ns during reset. Such unique PCM characteristics are enabled by the GST467 nanocomposite phase-change material described in our earlier work [13].

Behavioral models for potentiation and depression are constructed [**Figs. 1(b,c) insets**] using $\Delta G = \alpha \exp[-\beta(G_{max} - G)/(G_{max} - G_{min})]$ and $G_i = G_{i-1} \pm \Delta G_i + \delta\sigma_i$. Here, G_{max} and G_{min} are the maximum (200 μS) and the minimum (20 μS) conductance, respectively; α and β are fitting parameters,

Manuscript received 20 July 2024; accepted 3 August 2024. Date of publication 6 August 2024; date of current version 27 September 2024. This work was supported in part by the Semiconductor Research Corporation (SRC). The review of this letter was arranged by Editor S. Yu. *(Shafin Bin Hamid and Asir Intisar Khan contributed equally to this work.) (Corresponding author: Eric Pop.)*

Shafin Bin Hamid is with the Department of Electrical and Electronic Engineering, Bangladesh University of Engineering and Technology, West Palashi, Dhaka 1205, Bangladesh.

Asir Intisar Khan is with the Department of Electrical Engineering, Stanford University, Stanford, CA 94305 USA.

Huairuo Zhang and Albert V. Davydov are with the Materials Science and Engineering Division, National Institute of Standards and Technology, Gaithersburg, MD 20899 USA.

Eric Pop is with the Department of Electrical Engineering, Stanford University, Stanford, CA 94305 USA (e-mail: epop@stanford.edu).

Color versions of one or more figures in this letter are available at https://doi.org/10.1109/LED.2024.3439532.

Digital Object Identifier 10.1109/LED.2024.3439532

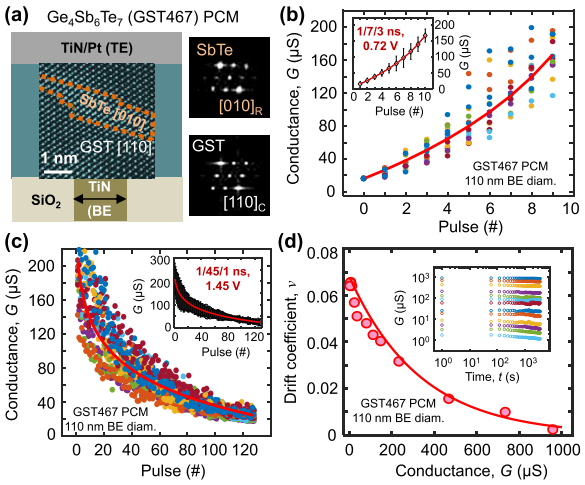

Fig. 1. **Device structure and electrical measurement.** **(a)** Schematic of a $Ge_4Sb_6Te_7$ (GST467) PCM device displaying an atomic-resolution STEM image of GST467 and corresponding FFT images of the SbTe nanocomposite and GST phases. **(b)** Evolution of conductance (**G**) states in GST467 PCM with number of pulses for potentiation (set), and **(c)** depression (reset) each for 15 different cycles in the same device. Red lines are fits using the behavioral model detailed in the main text. Error bars in the insets represent cycle-to-cycle variation at each pulse. More pulses are used for the depression cycle (c) to enable the larger (10x) conductance window. **(d)** Variation of conductance drift coefficient, ν for various conductance states in GST467 PCM. (Inset showing the measured conductance states over time, t). The red line represents a fit to the experimental data, as detailed in the main text.

i is the pulse number. To incorporate the cycle-to-cycle variation, we define σ_i as the standard deviation of the i^{th} conductance G_i, and δ as a random variable with a normal distribution of zero mean and unit variance. Conductance drift coefficient, υ for various conductance states [**Fig. 1(d)**] is modeled using $G = G_0 t^{-\upsilon}$ and $\upsilon = \alpha_d \exp(-\beta_d G)$, where G_0 is the initial conductance, G is the conductance at time t and α_d and β_d are fitting parameters.

III. Results and Discussion

A two-layer SNN is trained based on unsupervised STDP using the behavioral model of the GST467 PCM synapse. The SNN architecture with a *single*-GST467 PCM per synapse is shown in **Fig. 2(a)**, with each input having a connection to an output neuron. The red line denotes an inhibitory connection [14] between the output neurons. The network can be implemented in a crossbar fashion using building blocks displayed in **Fig. 2(a)**. At each junction of the crossbar, there is a GST467 PCM synapse in series with a selector and a leaky-integrate and fire (LIF) neuron [15] at the end of each column. For comparison, we also implemented an architecture with *two* GST467 PCMs per synapse, following [4]. In this scheme, both PCM devices per synapse use *only* their potentiation (set) behavior. The first PCM device controls the long-term potentiation, while the conductance difference between the two potentiating PCMs accounts for the long-term depression.

We now focus on our SNN architecture with *single*-GST467 PCM per synapse. During training, image pixels are converted into Poisson 'pre-spike' trains assuming the firing rate is proportional to the intensity of the pixel value (e.g., 32 Hz for maximum pixel value of 255). Each pre-spike is 35 mV with a time step of 5 ms. For pattern learning, we train the network using only one output neuron. As an example, the SNN is trained with subsequent images of the two digits: '7' and then '2', each for 1500 time steps. The images are obtained from the MNIST hand-written digit recognition data set [16]. Each time a spike is produced by the LIF neuron, a set and a reset pulse are sent out as a 'post' signal. For each input that spiked in the previous (next) time step, the connecting GST467 PCM synapse is potentiated (depressed).

The weights during pattern learning are shown in **Fig. 2(b)** with white (black) regions representing high (low) conductance of the PCM synapses at the given time stamps (25 ms to 7.5 s for digit '7', and 8 s to 15 s for digit '2'). The results illustrate the capability of a single neuron to learn and then forget features of different digits over time. In **Fig. 2(c)**, we also exhibit pattern learning of letters from the English alphabet underlining the robustness of the GST467 PCM synapse to different data sets.

We also performed online learning using an SNN based on GST467 PCM [**Fig. 2(d)**]. During online learning, we used 3000 digit images from the MNIST data set to train our SNN for three epochs (iterations); each image is shown after 100 pre-spike time steps. **Fig. 2(d)** also displays the trained weights (W, as the gray-scale color bar) after online learning with 10 neurons, delineating the capability of each neuron to learn the patterns of a particular digit. Thus, using a *single* GST467 PCM per synapse, our proposed SNN can achieve both online and pattern learning, which is otherwise difficult to achieve using traditional PCM based on GST225.

After the training phase, the 3000 images are presented again to label the neurons based on their highest average spikes produced per digit class. Subsequently, the neurons are grouped into clusters based on their assigned classes. During inference, an image is identified by the highest average number of spikes produced per cluster across all time steps. We derive the recognition rate of the trained SNN through inference on 500 digits. The total training energy ($E_{syn,trn}$) is calculated by summing over energies spent across each synapse for all applied pulses during the training period.

The recognition rate and synapse training energy, $E_{syn,trn}$, are shown in **Fig. 2(e)** for five independent trials. As the number of neurons (N) increases, the recognition rate increases, however at the expense of higher training energy. The standard deviation of the recognition rate across these trials for $N = 100$ is $\sim 3.4\%$ [**Fig. 2(e)**], originating from the cycle-to-cycle variation of the conductance states [**Fig. 1(b,c)**]. For a more complicated data set than MNIST, an additional 'read-verify' scheme may be required to maintain a high accuracy [17], [18] in our SNN.

We also compared the average synaptic inference energy per image ($E_{syn,inf}$) for an SNN with a *single* GST467 PCM per synapse vs. with *two* GST467 PCMs per synapse. Our analysis shows the single GST467 PCM outperforms its two PCM counterparts, with the former achieving $\sim 2.5\times$ lower inference energy [**Fig. 2(f)** and **2(g)**], and higher device density.

The presence of LIF neurons within the SNN may limit these energy and area benefits [19]. However, neurons with low-energy, nanoscale CMOS [20] or non-volatile memories [21], [22] can mitigate such limitations. Leveraging these advances in neuron implementation, we expect our single-PCM per synapse approach with *identical* pulses to

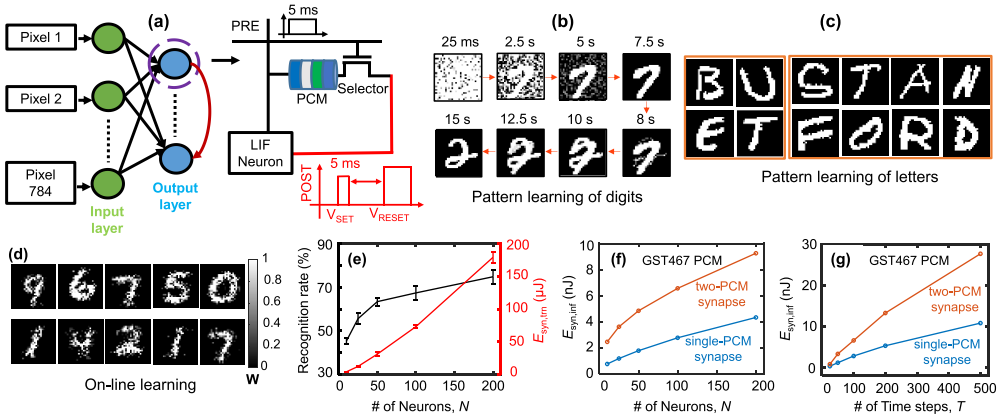

Fig. 2. **Spiking neural network (SNN) with GST467 PCM: (a)** Our designed SNN using GST467 PCM synapse. **(b)** Pattern learning of a neuron demonstrating the ability to learn and forget features of a digit over time. **(c)** Pattern learning of letters using GST467 synapses. **(d)** Online learning of 10 neurons trained on 3000 images. Color bar shows the range of weights W [0 1]. **(e)** Recognition rate (500 test images) and total training energy ($E_{syn,trn}$) for online learning (3000 training images) vs. the number of neurons (N). Error bars are derived from 5 different trials (representing cycle-to-cycle variation of the PCM synapse), causing an average ~3.4% variation in recognition rate, using trained weights from those trials. **(f)** Analysis of average inference energy ($E_{syn,inf}$) per image in synaptic communication, comparing one single PCM per synapse to two PCMs per synapse using GST467 PCM for varying number of neurons, N, and **(g)** varying number of time steps, T.

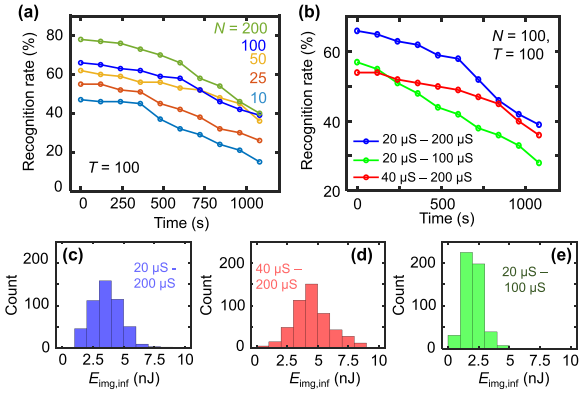

Fig. 3. **Impact of conductance drift on SNN behavior:** (a, b) Time evolution of SNN recognition rate reveals the effect of conductance drift in GST467 PCM. Results are shown for (a) variation in number of neurons (N) and **(b)** variation in conductance ranges used ($N = 100$ and number of time steps $T = 100$). **(c)** Energy spent in synapses during inference over 500 images for $N = 100$ neurons for a conductance range of 20 – 200 μS, **(d)** 40 – 200 μS, and **(e)** 20 – 100 μS.

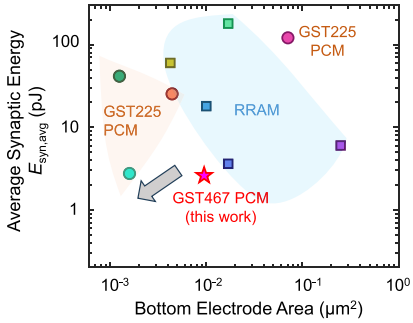

Fig. 4. **Benchmarking:** Average energy vs. BE area for synapses based on various resistive switching devices, e.g. resistive random-access memory (RRAM) [25], [26], [27], [28], [29] and PCM [1], [2], [3], [4], including the GST467 PCM in this work. Arrow marks the further reduction of $E_{syn,avg}$ expected with decreasing BE area.

maintain its advantages over the more complex two-PCM per synapse or single-PCM approach with *non-identical* pulses.

Next, we wish to understand the impact of conductance window and drift on both the accuracy and energy consumption of our SNN. Due to drift, the SNN recognition rate decreases over time for all N [**Fig. 3(a)**]. **Fig. 3(b)** shows that the recognition rate at $t = 0$ s (no drift) is higher for the larger conductance window (20 μS to 200 μS). For a fixed window of 5×, the recognition rate drops slowly for a higher conductance range (40 μS to 200 μS) than for a lower conductance range (20 μS to 100 μS). However, a higher conductance range, while beneficial for smaller drift, results in higher energy consumption during inference [**Figs. 3(c-e)**], revealing a trade-off between SNN recognition rate and energy consumption. We also find that to maintain high recognition accuracy, a refresh operation may be needed every ~250 s due to conductance drift [**Fig. 3(a)**]. While this does not significantly impact the $E_{syn,inf}$ during uninterrupted image inference, emerging phase-change superlattices and heterostructures with low drift [9], [23], [24] could be used to minimize these trade-offs in PCM-based SNN design.

Fig. 4 compares the GST467 PCM synapses in this work to various other synapses based on resistance switching from the literature. We estimated the average synaptic energy ($E_{syn,avg}$) of our GST467 PCM synapse by first summing the energies dissipated in the synapse for all the programming pulses (set, reset) during training and then dividing by the total number of programming pulses applied over the training duration. The $E_{syn,avg}$ vs. the bottom contact area shows the potential of the GST467 PCM synapse in energy-efficient and high-density SNN applications. With decreasing BE area, we expect a further reduction in the $E_{syn,avg}$, where the gradual potentiation and depression behaviors are expected to be maintained by the intrinsic properties of GST467.

IV. Conclusion

In summary, we present an energy-efficient spiking neural network (SNN) capable of both pattern and online learning with a *single* GST467 PCM per synapse. Our SNN shows ~2.5× lower inference energy compared to its *two*-PCM per synapse counterpart. We also find that PCM conductance drift causes a trade-off between recognition rate and energy consumption in such SNNs, thus drift should be carefully considered for their optimization and future implementation.

REFERENCES

[1] D. Kuzum, R. G. D. Jeyasingh, B. Lee, and H.-S.-P. Wong, "Nanoelectronic programmable synapses based on phase change materials for brain-inspired computing," *Nano Lett.*, vol. 12, no. 5, pp. 2179–2186, May 2012, doi: 10.1021/nl201040y.

[2] S. Ambrogio, N. Ciocchini, M. Laudato, V. Milo, A. Pirovano, P. Fantini, and D. Ielmini, "Unsupervised learning by spike timing dependent plasticity in phase change memory (PCM) synapses," *Frontiers Neurosci.*, vol. 10, p. 56, Mar. 2016, doi: 10.3389/fnins.2016.00056.

[3] B. L. Jackson, B. Rajendran, G. S. Corrado, M. Breitwisch, G. W. Burr, R. Cheek, K. Gopalakrishnan, S. Raoux, C. T. Rettner, A. Padilla, A. G. Schrott, R. S. Shenoy, B. N. Kurdi, C. H. Lam, and D. S. Modha, "Nanoscale electronic synapses using phase change devices," *ACM J. Emerg. Technol. Comput. Syst.*, vol. 9, no. 2, pp. 1–20, May 2013, doi: 10.1145/2463585.2463588.

[4] O. Bichler, M. Suri, D. Querlioz, D. Vuillaume, B. DeSalvo, and C. Gamrat, "Visual pattern extraction using energy-efficient '2-PCM synapse' neuromorphic architecture," *IEEE Trans. Electron Devices*, vol. 59, no. 8, pp. 2206–2214, Aug. 2012, doi: 10.1109/TED.2012.2197951.

[5] A. Sebastian, M. Le Gallo, and E. Eleftheriou, "Computational phase-change memory: Beyond von Neumann computing," *J. Phys. D, Appl. Phys.*, vol. 52, no. 44, Oct. 2019, Art. no. 443002, doi: 10.1088/1361-6463/ab37b6.

[6] A. I. Khan, A. Daus, R. Islam, K. M. Neilson, H. R. Lee, H.-S.-P. Wong, and E. Pop, "Ultralow-switching current density multilevel phase-change memory on a flexible substrate," *Science*, vol. 373, no. 6560, pp. 1243–1247, Sep. 2021, doi: 10.1126/science.abj1261.

[7] J. Shen, S. Lv, X. Chen, T. Li, S. Zhang, Z. Song, and M. Zhu, "Thermal barrier phase change memory," *ACS Appl. Mater. Interfaces*, vol. 11, no. 5, pp. 5336–5343, Feb. 2019, doi: 10.1021/acsami.8b18473.

[8] P.-Y. Chen, B. Lin, I.-T. Wang, T.-H. Hou, J. Ye, S. Vrudhula, J.-S. Seo, Y. Cao, and S. Yu, "Mitigating effects of non-ideal synaptic device characteristics for on-chip learning," in *Proc. IEEE/ACM Int. Conf. Comput.-Aided Design (ICCAD)*, Nov. 2015, pp. 194–199, doi: 10.1109/ICCAD.2015.7372570.

[9] X. Wu, A. I. Khan, P. Ramesh, C. Perez, K. Kim, Z. Lee, K. Saraswat, K. E. Goodson, H.-S. P. Wong, and E. Pop, "Understanding interface-controlled resistance drift in superlattice phase change memory," *IEEE Electron Device Lett.*, vol. 43, no. 10, pp. 1669–1672, Oct. 2022, doi: 10.1109/LED.2022.3203971.

[10] S. Oh, Z. Huang, Y. Shi, and D. Kuzum, "The impact of resistance drift of phase change memory (PCM) synaptic devices on artificial neural network performance," *IEEE Electron Device Lett.*, vol. 40, no. 8, pp. 1325–1328, Aug. 2019, doi: 10.1109/LED.2019.2925832.

[11] Y. Shi, Z. Huang, S. Oh, N. Kaslan, J. Song, and D. Kuzum, "Adaptive quantization as a device-algorithm co-design approach to improve the performance of in-memory unsupervised learning with SNNs," *IEEE Trans. Electron Devices*, vol. 66, no. 4, pp. 1722–1728, Apr. 2019, doi: 10.1109/TED.2019.2898402.

[12] M. Suri, O. Bichler, D. Querlioz, B. Traoré, O. Cueto, L. Perniola, V. Sousa, D. Vuillaume, C. Gamrat, and B. DeSalvo, "Physical aspects of low power synapses based on phase change memory devices," *J. Appl. Phys.*, vol. 112, no. 5, p. 54904, Sep. 2012, doi: 10.1063/1.4749411.

[13] A. I. Khan, H. Yu, H. Zhang, J. R. Goggin, H. Kwon, X. Wu, C. Perez, K. M. Neilson, M. Asheghi, K. E. Goodson, P. M. Vora, A. Davydov, I. Takeuchi, and E. Pop, "Energy efficient neuro-inspired phase–change memory based on $Ge_4Sb_6Te_7$ as a novel epitaxial nanocomposite," *Adv. Mater.*, vol. 35, no. 30, Jul. 2023, Art. no. 2300107, doi: 10.1002/adma.202300107.

[14] P. U. Diehl and M. Cook, "Unsupervised learning of digit recognition using spike-timing-dependent plasticity," *Frontiers Comput. Neurosci.*, vol. 9, p. 99, Aug. 2015, doi: 10.3389/fncom.2015.00099.

[15] S. Dutta, V. Kumar, A. Shukla, N. R. Mohapatra, and U. Ganguly, "Leaky integrate and fire neuron by charge-discharge dynamics in floating-body MOSFET," *Sci. Rep.*, vol. 7, no. 1, p. 8257, Aug. 2017, doi: 10.1038/s41598-017-07418-y.

[16] L. Deng, "The MNIST database of handwritten digit images for machine learning research," *IEEE Signal Process. Mag.*, vol. 29, no. 6, pp. 141–142, Nov. 2012, doi: 10.1109/MSP.2012.2211477.

[17] N. Papandreou, H. Pozidis, A. Pantazi, A. Sebastian, M. Breitwisch, C. Lam, and E. Eleftheriou, "Programming algorithms for multilevel phase-change memory," in *Proc. IEEE Int. Symp. Circuits Syst. (ISCAS)*, May 2011, pp. 329–332, doi: 10.1109/ISCAS.2011.5937569.

[18] S. Oh, Y. Shi, X. Liu, J. Song, and D. Kuzum, "Drift-enhanced unsupervised learning of handwritten digits in spiking neural network with PCM synapses," *IEEE Electron Device Lett.*, vol. 39, no. 11, pp. 1768–1771, Nov. 2018, doi: 10.1109/LED.2018.2872434.

[19] G. Indiveri, E. Chicca, and R. Douglas, "A VLSI array of low-power spiking neurons and bistable synapses with spike-timing dependent plasticity," *IEEE Trans. Neural Netw.*, vol. 17, no. 1, pp. 211–221, Jan. 2006, doi: 10.1109/TNN.2005.860850.

[20] T. Chavan, S. Dutta, N. R. Mohapatra, and U. Ganguly, "Band-to-band tunneling based ultra-energy-efficient silicon neuron," *IEEE Trans. Electron Devices*, vol. 67, no. 6, pp. 2614–2620, Jun. 2020, doi: 10.1109/TED.2020.2985167.

[21] T. Tuma, A. Pantazi, M. Le Gallo, A. Sebastian, and E. Eleftheriou, "Stochastic phase-change neurons," *Nature Nanotechnol.*, vol. 11, no. 8, pp. 693–699, Aug. 2016, doi: 10.1038/nnano.2016.70.

[22] A. Dongre and G. Trivedi, "RRAM-based energy efficient scalable integrate and fire neuron with built-in reset circuit," *IEEE Trans. Circuits Syst. II, Exp. Briefs*, vol. 70, no. 3, pp. 909–913, Mar. 2023, doi: 10.1109/TCSII.2022.3219203.

[23] K. Ding, J. Wang, Y. Zhou, H. Tian, L. Lu, R. Mazzarello, C. Jia, W. Zhang, F. Rao, and E. Ma, "Phase-change heterostructure enables ultralow noise and drift for memory operation," *Science*, vol. 366, no. 6462, pp. 210–215, Oct. 2019, doi: 10.1126/science.aay0291.

[24] A. I. Khan, X. Wu, C. Perez, B. Won, K. Kim, P. Ramesh, H. Kwon, M. C. Tung, Z. Lee, I.-K. Oh, K. Saraswat, M. Asheghi, K. E. Goodson, H.-S.-P. Wong, and E. Pop, "Unveiling the effect of superlattice interfaces and intermixing on phase change memory performance," *Nano Lett.*, vol. 22, no. 15, pp. 6285–6291, Aug. 2022, doi: 10.1021/acs.nanolett.2c01869.

[25] A. Valentian, F. Rummens, E. Vianello, T. Mesquida, C. L. de Boissac, O. Bichler, and C. Reita, "Fully integrated spiking neural network with analog neurons and RRAM synapses," in *IEDM Tech. Dig.*, Dec. 2019, pp. 14.3.1–14.3.4, doi: 10.1109/IEDM19573.2019.8993431.

[26] S. H. Jo, T. Chang, I. Ebong, B. B. Bhadviya, P. Mazumder, and W. Lu, "Nanoscale memristor device as synapse in neuromorphic systems," *Nano Lett.*, vol. 10, no. 4, pp. 1297–1301, Apr. 2010, doi: 10.1021/nl904092h.

[27] S. Yu, Y. Wu, R. Jeyasingh, D. Kuzum, and H.-S. P. Wong, "An electronic synapse device based on metal oxide resistive switching memory for neuromorphic computation," *IEEE Trans. Electron Devices*, vol. 58, no. 8, pp. 2729–2737, Aug. 2011, doi: 10.1109/TED.2011.2147791.

[28] T. Werner, E. Vianello, O. Bichler, D. Garbin, D. Cattaert, B. Yvert, B. De Salvo, and L. Perniola, "Spiking neural networks based on OxRAM synapses for real-time unsupervised spike sorting," *Frontiers Neurosci.*, vol. 10, p. 474, Nov. 2016, doi: 10.3389/fnins.2016.00474.

[29] A. Regev, A. Bricalli, G. Piccolboni, A. Valentian, T. Mesquida, G. Molas, and J.-F. Nodin, "Fully-integrated spiking neural network using SiOx-based RRAM as synaptic device," in *Proc. 2nd IEEE Int. Conf. Artif. Intell. Circuits Syst. (AICAS)*, Aug. 2020, pp. 145–148, doi: 10.1109/AICAS48895.2020.9073840.